

Interaction between chiral ions: synthesis and characterization of tartratovanadates(V) with tris(2,2'-bipyridine) complexes of iron(II) and nickel(II) as cations

Peter Antal · Peter Schwendt · Jozef Tatiersky ·
Róbert Gyepes · Milan Drábik

Received: 26 June 2014 / Accepted: 16 August 2014 / Published online: 26 August 2014
© Springer International Publishing Switzerland 2014

Abstract Four new compounds composed of chiral complex cations and anions: Δ -[Fe(*bpy*)₃] Λ -[Fe(*bpy*)₃][V₄O₈((2*R*,3*R*)-*tart*)₂]·12H₂O (**1**), Δ -[Fe(*bpy*)₃]₂ Λ -[Fe(*bpy*)₃]₂[V₄O₈((2*R*,3*R*)-*tart*)₂][V₄O₈((2*S*,3*S*)-*tart*)₂]·24H₂O (**2**), Δ -[Ni(*bpy*)₃] Λ -[Ni(*bpy*)₃][V₄O₈((2*R*,3*R*)-*tart*)₂]·12H₂O (**3**) and Δ -[Ni(*bpy*)₃]₂ Λ -[Ni(*bpy*)₃]₂[V₄O₈((2*R*,3*R*)-*tart*)₂][V₄O₈((2*S*,3*S*)-*tart*)₂]·24H₂O (**4**) have been prepared. The compounds have been characterized by spectral methods, and their thermal decomposition was studied by simultaneous DTA, TG measurements. The final products after dynamic decomposition and additional heating were Fe₂V₄O₁₃ for **1** and **2** and Ni(VO₃)₂ for **3** and **4**. The crystal structures determined for **1**, **2** and **4** have evidenced that **1** is “hemiracemic” and **2** and **4** are “fully racemic” compounds.

Introduction

The interaction of chiral cations with chiral anions or chiral cations (anions) with achiral anions (cations) in solution

P. Antal · P. Schwendt · J. Tatiersky (✉) · M. Drábik
Department of Inorganic Chemistry, Faculty of Natural Sciences,
Comenius University, Mlynská dolina, 842 15 Bratislava,
Slovak Republic
e-mail: tatiersky@fns.uniba.sk

R. Gyepes
Faculty of Education, J. Selye University, Bratislavská cesta
3322, 945 01 Komárno, Slovak Republic

R. Gyepes
J. Heyrovský Institute of Physical Chemistry of the AS CR,
v.v.i., Dolejškova 3, 182 23 Prague 8, Czech Republic

M. Drábik
Institute of Inorganic Chemistry, Slovak Academy of Sciences,
Dúbravská cesta 9, 845 36 Bratislava 45, Slovak Republic

may lead to crystallization of a conglomerate, racemic compound or eventually to concomitant crystallization of both compound types [1–7]. The kind of products obtained depends on the type of forces operating in the crystal structure. Besides electrostatic interactions, various weak interactions (H-bonds, π - π , cation- π , anion- π interactions) can influence the results of crystallization; the interplay of very fine effects often determines the kind of crystals [1–6]. Even in the case of crystallization of racemic compounds, some homochiral parts of crystals (chains, layers) can be formed, and preferred interactions between the chiral ions can be observed. Thus, in the case of $[M(bpy)_3][VO(O_2)(ox)(bpy)]_2$ compounds ($M = Fe, Ni$; $ox = C_2O_4^{2-}$), we observed the preference of Δ - $[M(bpy)_3]^{2+}$ - A - $[VO(O_2)(ox)(bpy)]^-$ and Λ - $[M(bpy)_3]^{2+}$ - B - $[VO(O_2)(ox)(bpy)]^-$ interactions (A and B denote different enantiomers of the anion), which resulted in formation of homochiral layers [7].

Tartaric acid and its derivatives are often used as resolving agents, and to continue our previous studies on interaction of chiral $[M(bpy)_3]^{2+}$ cations with various chiral anions, we decided to study their interaction with anionic vanadium tartrato complexes. Here we present the characterization of products crystallizing from solutions containing *rac*- $[M(bpy)_3]^{2+}$ and chiral tartrato complexes of vanadium(V). In all cases, racemic or hemiracemic compounds were obtained.

Experimental

Chemicals

KVO₃ was prepared by reaction of an aqueous solution of KOH with V₂O₅ [7]. V₂O₅ was prepared as follows.

All other chemicals used were of reagent grade and used without further purification.

Preparation of V_2O_5

Ammonium vanadate (50.0 g) was purified by dissolving in an aqueous solution of ammonia ($w = 26\%$, 60.0 mL) and water (1.50 L). The obtained solution was heated to 60 °C, filtered and cooled in air to ambient temperature. Ammonium nitrate (70.0 g) was then added. A white precipitate was obtained (NH_4VO_3), which was filtered off and washed with cold water (20.0 mL) and then ethanol (20.0 mL). V_2O_5 was prepared by thermal decomposition (2 h at 500 °C) of purified ammonium vanadate. The purity of vanadium pentoxide was verified by powder XRD and reductometric determination of vanadium [8].

Synthesis of Δ -[Fe(*bpy*)₃] Λ -[Fe(*bpy*)₃][V₄O₈((2*R*,3*R*)-*tart*)₂] \cdot 12H₂O (**1**)

Potassium vanadate (138 mg; 1.00 mmol) was dissolved in water (10.0 mL). After the addition of solid (2*R*,3*R*)-tartaric acid (76.6 mg, 0.50 mmol), a red solution was obtained. To this solution, another solution of iron(II) sulfate heptahydrate (139 mg, 0.50 mmol) and 2,2'-bipyridine (234 mg, 1.5 mmol) in aqueous ethanol ($\varphi = 24\%$, 20.0 mL) was added. The solution obtained was allowed to crystallize at 5 °C. Dark red crystals were isolated after 2 weeks and dried at 5 °C. Anal. Calc. for C₆₈H₇₆N₁₂O₃₂V₄Fe₂: C, 43.2; H, 4.1; N, 8.9. Found: C, 42.8; H, 3.9; N, 8.6.

Synthesis of Δ -[Fe(*bpy*)₃]₂ Λ -[Fe(*bpy*)₃]₂[V₄O₈((2*R*,3*R*)-*tart*)₂][V₄O₈((2*S*,3*S*)-*tart*)₂] \cdot 24H₂O (**2**)

Potassium vanadate (139 mg; 1.00 mmol) was dissolved in water (10.0 mL), and racemic tartaric acid (76.5 mg; 0.50 mmol) was added. To the red solution obtained, another solution of iron(II) sulfate heptahydrate (139 mg; 0.50 mmol) and 2,2'-bipyridine (234 mg, 1.5 mmol) in ethanol (5.0 mL), water (20.0 mL) and acetonitrile (5 mL) was added. The solution was allowed to crystallize at 5 °C. Dark red crystals were isolated after 3 weeks. Anal. Calc. for C₆₈H₇₆N₁₂O₃₂V₄Fe₂: C, 43.2; H, 4.1; N, 8.9. Found: C, 42.2; H, 3.6; N, 9.2.

Synthesis of Δ -[Ni(*bpy*)₃] Λ -[Ni(*bpy*)₃][V₄O₈((2*R*,3*R*)-*tart*)₂] \cdot 12H₂O (**3**)

Potassium vanadate (138 mg; 1.00 mmol) was dissolved in water (10.0 mL), and solid (2*R*,3*R*)-tartaric acid (75 mg; 0.50 mmol) was added. To the red solution obtained, another solution of nickel(II) chloride hexahydrate

(119 mg, 0.50 mmol) and 2,2'-bipyridine (234 mg, 1.50 mmol) in ethanol ($\varphi = 48\%$, 10.0 mL) was added. The obtained solution was filtered and allowed to crystallize at 5 °C. Orange crystals were isolated after 12 h and dried at 5 °C. The obtained crystals were not suitable for structural analysis. Anal. Calc. for C₆₈H₇₆N₁₂O₃₂V₄Ni₂: C, 43.1; H, 4.0; N, 8.9. Found: C, 42.1; H, 3.8; N, 8.6.

Synthesis of Δ -[Ni(*bpy*)₃]₂ Λ -[Ni(*bpy*)₃]₂[V₄O₈((2*R*,3*R*)-*tart*)₂][V₄O₈((2*S*,3*S*)-*tart*)₂] \cdot 24H₂O (**4**)

Potassium vanadate (276 mg; 2.00 mmol) was dissolved in water (15.0 mL). After the addition of solid racemic tartaric acid (300 mg, 2.00 mmol), a red solution was obtained. To this solution, another solution of nickel(II) chloride hexahydrate (237 mg, 1.00 mmol) and 2,2'-bipyridine (469 mg, 3.00 mmol) in ethanol ($\varphi = 48\%$, 10.0 mL) was added. The solution obtained was filtered and allowed to crystallize at 5 °C. Orange crystals were isolated after 12 h and dried at 5 °C. Anal. Calc. for C₆₈H₇₆N₁₂O₃₂V₄Ni₂: C, 43.1; H, 4.0; N, 8.9. Found: C, 43.1; H, 4.0; N, 8.7.

Methods and instrumentation

Elemental analyses (C, H, N) were performed on a Vario MIKRO cube (Elementar). IR spectra were recorded on an FTIR Nicolet 6700 spectrometer in Nujol mulls and KBr discs. The ⁵¹V NMR spectra of aqueous solutions were registered at 278 K on a Varian Mercury Plus 300 MHz spectrometer operating at 78.94 MHz (⁵¹V) in 5-mm tubes without locking on D₂O and 30 min after dissolution. Chemical shifts are related to VOCl₃ as an external standard. Electronic spectra of aqueous solutions were measured in range 200–1,000 nm on a Jasco V-530 (Shimadzu) apparatus in 1-cm quartz cuvettes at room temperature. The spectra were measured 10 min after dissolution. Powder X-ray diffraction patterns were obtained on a PANalytical Empyrean diffractometer using CuK_α radiation ($\lambda = 1.5406$ Å) with Bragg–Brentano arrangement. DTA and TG curves were measured on SDT 2960 (TA Instruments) apparatus in air in the temperature range 20–500 °C with the heating rate 10 °C min⁻¹.

X-ray data collection and structure refinement

Diffraction data were collected at 150(2) K on a Nonius KappaCCD diffractometer (MoK_α radiation, $\lambda = 0.71073$ Å) equipped with a Bruker APEX-II CCD detector and processed using the software package delivered with the diffractometer. Diffraction data were corrected employing a symmetry-related (multi-scan) absorption

Table 1 Crystal data and structure refinement for **1**, **2** and **4** (formulas of compounds are normalized as crystallographic formula units)

Compound	1	2	4
Formula	C ₆₈ H ₇₆ N ₁₂ O ₃₂ V ₄ Fe ₂	C ₆₈ H ₇₆ N ₁₂ O ₃₂ V ₄ Fe ₂	C ₆₈ H ₇₆ N ₁₂ O ₃₂ V ₄ Ni ₂
<i>M_r</i>	1,888.87	1,888.87	1,894.59
Crystal system	Monoclinic	Monoclinic	Monoclinic
Space group	<i>P</i> 2 ₁ (no. 4)	<i>P</i> 2 ₁ / <i>c</i> (no. 14)	<i>P</i> 2 ₁ / <i>c</i> (no. 14)
<i>a</i> (Å)	23.4634(6)	24.2609(10)	24.3341(8)
<i>b</i> (Å)	13.6462(3)	13.9399(5)	14.5312(5)
<i>c</i> (Å)	24.5395(7)	23.382(1)	23.3803(9)
β (°)	90.422(1)	99.023(2)	99.611(1)
Volume (Å ³)	7,857.0(3)	7,809.8(5)	8,151.3(5)
<i>Z</i>	4	4	4
<i>R</i> ₁ ^{a,b}	0.0478	0.0399	0.0393
<i>wR</i> ₂ ^c	0.1072	0.0943	0.0991
<i>R</i> ₁ (all data)	0.0672	0.0518	0.0533

^a $I > 2\sigma(I)$ ^b $R_1 = 100 \sum(|F_o| - |F_c|) / \sum |F_o|$ ^c $wR_2 = 100 [\sum [w(F_o^2 - F_c^2)^2] / \sum [w(F_o^2)]^{1/2}, w = 1 / [\sigma^2(F_o^2) + [(ap)^2 + bp]]]$, where $p = [\max(F_o^2, 0) + 2F_c^2] / 3$, *a* and *b* are constants

correction. All non-hydrogen atoms were refined anisotropically; hydrogen atoms were included in their ideal positions and refined isotropically. Solvent molecules could not be refined satisfactorily in either case and have been removed from the final model using the SQUEEZE procedure as implemented in Platon [9]. A disorder of one *tart* ligand in **2** and **4** was treated by constraining the sum of site occupancy factors of the two moieties located on difference Fourier maps. An analogous approach was used to resolve the other disorder of **2**, which had one of its *bpy* ligands struck by a similar division into two positions. Crystal data and final refinement parameters are given in Table 1.

Results and discussion

Syntheses and spectroscopic studies

Compounds **1–4** were prepared by crystallization from the KVO₃–tartaric acid–FeSO₄·7H₂O (NiCl₂·6H₂O)–2,2′-bipyridine–H₂O–ethanol–(acetonitrile) systems. The compounds are moderately soluble in water under partial decomposition (vide infra). The solid complexes are relatively stable, as they can be stored at 5 °C at least for 1 week without decomposition. Compounds **1–4** are moderately soluble in water and insoluble in acetonitrile.

The infrared spectra of **1–4** (Table 2) exhibit characteristic bands of the $[M(bpy)_3]^{2+}$ cations and tetranuclear $[V_4O_8(tart)_2]^{4-}$ anions. The strong bands corresponding to stretching vibrations, in plane and out of plane bending vibrations of the 2,2′-bipyridine rings, can be observed in expected positions [10]. For the $[V_4O_8(tart)_2]^{4-}$ anions especially the bands which can be assigned to $\nu_{as}(\text{COO}^-)$, $\nu_s(\text{COO}^-)$, $\nu(\text{V}=\text{O}_i)$ and $\nu(\text{VOV})$ vibrations are characteristic [11]. For all of the complexes studied here, the difference between the asymmetric and symmetric stretches

was $>250 \text{ cm}^{-1}$, indicating that the carboxylate groups in the tartrate ligand are coordinated to vanadium in a monodentate fashion [12]. The infrared spectra of **1–4** exhibit a mutual similarity—only small differences can be observed for $\nu_s(\text{COO}^-)$ and $\nu(\text{V}=\text{O}_h)$ vibrations (Table 2).

The ⁵¹V NMR spectra of all compounds exhibit two dominant signals (Fig. 1): a signal at approximately –523 ppm corresponding to $[V_4O_8(tart)_2]^{4-}$ (–524 ppm, *I*_{rel} = 72 % for **1**; –521 ppm, *I*_{rel} = 67 % for **2**; –524 ppm, *I*_{rel} = 77 % for **3**; –523 ppm, *I*_{rel} = 68 % for **4**) and another at –539 ppm corresponding to $[V_2O_4(\text{H}_2\text{tart})_2]^{2-}$ (–540 ppm, *I*_{rel} = 28 % for **1**; –536 ppm, *I*_{rel} = 33 % for **2**; –539 ppm, *I*_{rel} = 23 % for **3**; –539 ppm, *I*_{rel} = 32 % for **4**) [11].

The UV–Vis spectra of **1–4** are dominated by the absorption bands of the cations. Therefore, we discuss here only the spectra of **1** and **4** (Figs. 2, 3). Electronic spectra of **1** and **4** exhibit in the UV-region below 320 nm bands corresponding to the intraligand (*bpy*) $\pi \rightarrow \pi^*$ transitions [13, 14]. In the spectrum of **1**, the characteristic MLCT [13, 15] bands were observed at 347, 491 and 522 nm, which account for the typical red color of the Fe(II)-*tris*(diimine) complexes (Table 3). The *d–d* transitions give rise to three bands in the spectrum of **4**. The lowest energy band is in agreement with literature data [14, 16] assigned to the spin forbidden transition $^3A_{2g} \rightarrow ^1E_g$. The third spin allowed *d–d* band [$^3A_{2g} \rightarrow ^3T_{1g}(\text{P})$] in the spectrum of **1** is supposed to be below 330 nm and is hidden behind the very strong $\pi \rightarrow \pi^*$ bands.

The TG curves of **1–4** show several overlapping decomposition steps without any distinct plateaus. The first step on the TG curves of **1** and **2** (Fig. 4, because of similarity of both TG curves only the curve of **2** is depicted) accompanied by an endothermic peak on the DTA curve at about 100 °C was assigned predominantly to the release of crystal water (calc. weight loss 11.45 %, found 13.02 % and 9.22 % for **1** and **2**, respectively). The next step on the TG curves with a corresponding exothermic maximum on the DTA curve at ≈ 190 °C was attributed mostly to the

Table 2 Infrared spectra of **1–4** (1,700–400 cm⁻¹)

1	2	3	4	Assignment
1,624 vs	1,624 vs	1,631 s	1,628 vs	$\nu_{\text{as}}(\text{COO}^-)$
1,603 vs	1,602 vs	1,605 vs		$\nu(\text{ring})$
		1,598 vs	1,597 vs	$\nu(\text{ring})$
		1,575 m	1,574 w	$\nu(\text{ring})$
1,568 sh	1,568 sh	1,568 sh	1,566 sh	$\nu(\text{ring})$
1,467 s	1,466 m	1,493 w	1,492 m	$\nu(\text{ring})$
		1,473 m	1,472 m	$\nu(\text{ring})$
1,443 s	1,443 s	1,443 vs	1,442 vs	$\nu(\text{ring})$
1,427 m	1,426 m			$\nu(\text{ring})$
1,358 m	1,363 m	1,369 w	1,347 m	$\nu_{\text{s}}(\text{COO}^-)$
1,313 m	1,314 m	1,314 m	1,314 m	$\nu(\text{ring})$
1,271 w	1,271 w	1,283 w		$\nu(\text{ring})$
1,242 w	1,241 w	1,247 w	1,247 m	$\alpha(\text{C-H})$
1,229 w	1,226 w	1,226 w	1,224 w	$\nu(\text{ring})$
1,173 w	1,172 w	1,176 w	1,175 m	$\alpha(\text{C-H})$
1,161 w	1,160 w	1,160 m	1,158 m	$\alpha(\text{C-H})$
1,092 m	1,091 m	1,090 m	1,092 m	$\nu(\text{C-O}_h)$
1,067 w	1,065 m	1,064 w	1,063 w	$\nu(\text{C-O}_h)$
	1,045 w	1,045 w	1,045 w	$\nu(\text{ring})$
		1,021 s	1,022 m	$\nu(\text{ring})$
963 s	960 s	963 s	962 vs	$\nu(\text{V=O}_t)$
918 sh	920 w	916 w	918 w	$\nu(\text{C}_{\text{tart}}-\text{C}_{\text{tart}})$
850 m	849 m	848 m	849 m	$\delta(\text{COO})$
822 m	822 m	819 sh	823 w	$\delta(\text{COO})$
775 vs	775 vs	778 vs	775 vs	$\gamma(\text{ring})$
752 sh	754 sh			$\nu_{\text{as}}(\text{VOV})$
735 s	734 s	738 s	737 vs	$\gamma(\text{C-H})$
659 m	660 m		663 sh	$\nu(\text{ring})$
648 w	649 m	653 m	653 m	$\nu(\text{ring})$
551 s	547 s	548 m	552 s	$\nu_{\text{s}}(\text{VOV})$
515 sh	513 w	530 sh	514 m	$\nu(\text{V-O}_h)$
		497 w	486 w	$\nu(\text{V-O}_h)$
435 m	434 m	439 m	436 m	$\gamma(\text{ring})$
409 w	409 w	420 w	417 w	$\gamma(\text{ring})$

ν Stretching, δ bending, α in plane bending, γ out of plane bending, O_t terminal oxygen atom, O_h oxygen atom from deprotonated hydroxyl group of tartrate ligand, C_{tart} carbon atom from tartrate ligand

decomposition of the tartrate ligand. The following steps on the TG curves accompanied by several exothermic peaks on the DTA curves were assigned to the decomposition of $[\text{Fe}(\text{bpy})_3]^{2+}$ cation, which exhibits a considerable thermal stability [17] while undergoing a simultaneous oxidation of $\text{Fe}^{\text{II}}-\text{Fe}^{\text{III}}$.

The final product of dynamic decomposition, according to the IR spectra and powder X-ray diffraction patterns, is a mixture of V_2O_5 and FeVO_4 including a small admixture of $\text{Fe}_2\text{V}_4\text{O}_{13}$. According to IR and X-ray diffraction, the prolonged heating of **1** and **2** (24 h) at 620 °C afforded

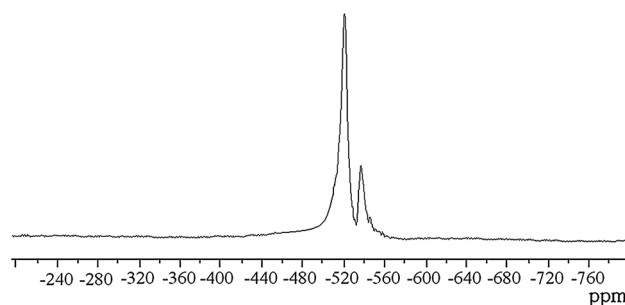
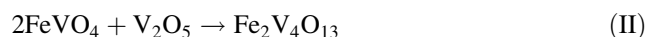
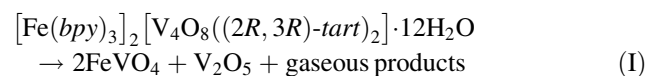


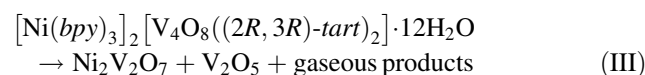
Fig. 1 ^{51}V NMR spectra of aqueous solution of **3** ($c = 1 \times 10^{-4}$ mol/L)

nearly pure $\text{Fe}_2\text{V}_4\text{O}_{13}$ [18]. The whole process of the thermal decomposition of **1** and **2** is described by Schemes I and II (calc. total weight loss 71.61 %, found 72.76 % for **1** and 72.30 % for **2**).



The TG curves of **3** and **4** (Fig. 5; because of the similarity of both TG curves only that of **4** is depicted) exhibit some similarities with the TG curves of **1** and **2**. We can propose the release of crystal water (endothermic peak at ≈ 100 °C, calc. weight loss 11.43 %, found 11.56 % for **3** and 8.58 % for **4**). Three exothermic effects on the DTA curves at ≈ 197 , ≈ 260 and ≈ 395 °C correspond to the decomposition of organic ligands.

The whole decomposition process is expressed by Schemes III and IV (calc. total weight loss 72.86 %, found 73.24 % for **3** and 72.11 % for **4**).



The products of decomposition given in Schemes III and IV were confirmed by X-ray powder patterns and IR spectra [19, 20]. The final product of dynamic decomposition was $\text{Ni}(\text{VO}_3)_2$ including a small admixture of V_2O_5 and $\text{Ni}_2\text{V}_2\text{O}_7$. After additional heating of this mixture (580 °C, 3 h), pure $\text{Ni}(\text{VO}_3)_2$ was obtained.

A nicely differentiated IR spectrum of $\text{Ni}(\text{VO}_3)_2$, to the best of our knowledge unpublished so far, is presented in Fig. 6. The rich spectrum in the range of V–O stretching vibrations corresponds to variability of the V–O bond lengths found in the structure [21].

Description of the crystal structures

Crystallization from solution containing both enantiomers of the cation and anion can lead to different types of products (Fig. 7). The most common crystallization product

Fig. 2 Electronic spectrum of aqueous solution of **1** ($c = 1 \times 10^{-5}$ mol/L)

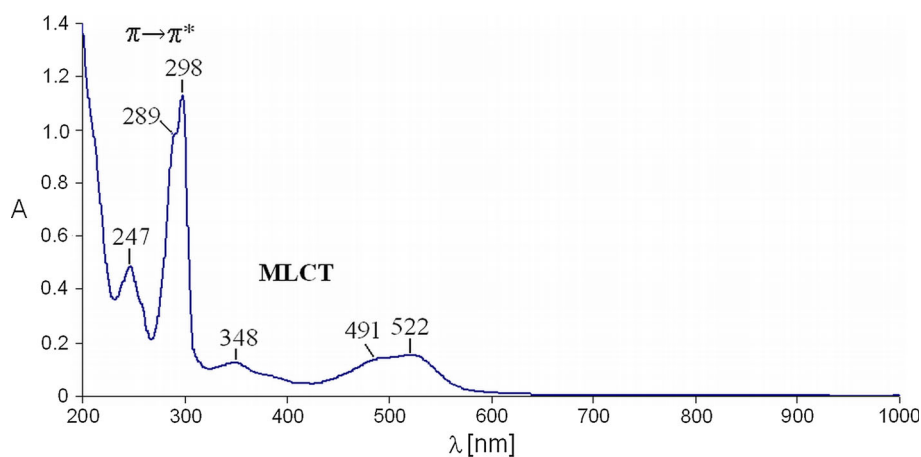


Fig. 3 Electronic spectra of aqueous solutions of **4** measured at various concentrations: 7.4×10^{-6} mol/L (**a**) and 4.7×10^{-4} mol/L (**b, c**) (the concentrations are based on chemical formula given in Table 1)

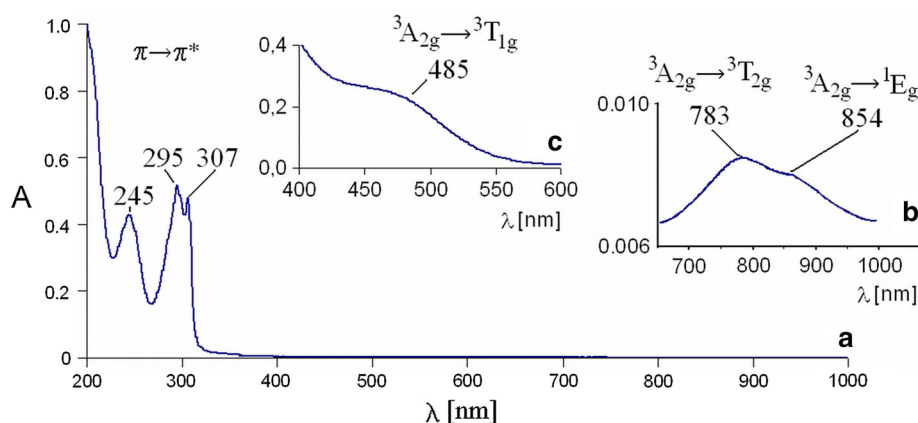


Table 3 Electronic spectral data of aqueous solutions of **1** and **4**

λ (nm)	ε (L mol ⁻¹ cm ⁻¹)	Assignment
[Fe(<i>bpy</i>) ₃] ₂ [V ₄ O ₈ ((2 <i>R</i> ,3 <i>R</i>)- <i>tart</i>) ₂] ₂ ·12H ₂ O (1) ($c = 1 \times 10^{-5}$ mol/L)		
247	4.8×10^4	$\pi \rightarrow \pi^*$
289	9.7×10^4	$\pi \rightarrow \pi^*$
298	1.1×10^5	$\pi \rightarrow \pi^*$
348	1.2×10^4	MLCT
491	1.4×10^4	MLCT
522	1.5×10^4	MLCT
[Ni(<i>bpy</i>) ₃] ₄ [V ₄ O ₈ ((2 <i>R</i> ,3 <i>R</i>)- <i>tart</i>) ₂][V ₄ O ₈ ((2 <i>R</i> ,3 <i>R</i>)- <i>tart</i>) ₂] ₂ ·24H ₂ O (4) ^a		
245	5.7×10^4	$\pi \rightarrow \pi^*$
295	7.0×10^4	$\pi \rightarrow \pi^*$
307	6.4×10^4	$\pi \rightarrow \pi^*$
485	sh	${}^3A_{2g} \rightarrow {}^3T_{1g}$ (F)
783	35	${}^3A_{2g} \rightarrow {}^3T_{2g}$
854	sh	${}^3A_{2g} \rightarrow {}^1E_g$

Values of ε were calculated using chemical formulas given in Table 1

^a Electronic spectra of compound **4** were measured at different concentrations: 7.4×10^{-6} mol/L (bands: 245, 295, 307 nm) and 4.7×10^{-4} mol/L (bands 485 sh, 783, 854 sh nm)

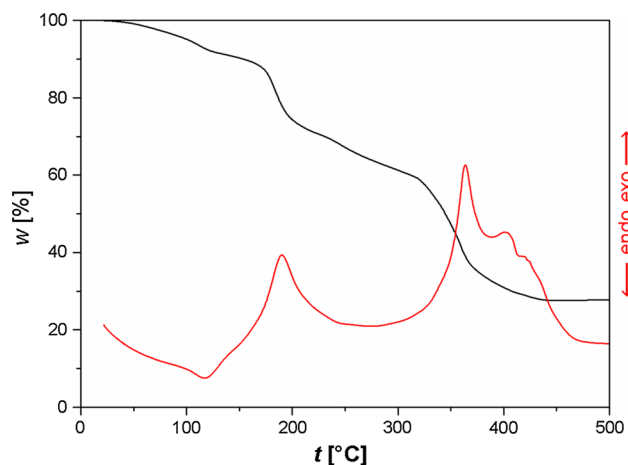


Fig. 4 TG and DTA curves of **2**

(approximately 90 % of products) is a racemic compound containing both enantiomers of cations and anions in equal amount in its crystal structure. The other type is a racemic conglomerate (approximately 10 % of products). Sometimes (generally very rarely), racemic compound and

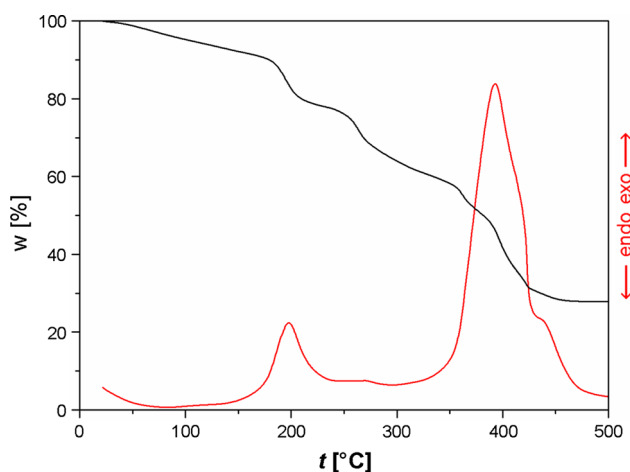


Fig. 5 TG and DTA curves of **4**

racemic conglomerate crystallize concomitantly [7, 22]. Racemic conglomerates can be divided into two types: Crystals of the first type contain only one enantiomer both of cations and anions, while crystals of the second type are composed of one enantiomer of cation (anion) and both enantiomers of anion (cation) (“hemiracemic” compound).

The tetranuclear anions $[V_4O_8(tart)_2]^{4-}$ in **1**, **2** and **4** (Fig. 8) consist of one $\{V_4O_8\}$ group and two (2*R*,3*R*)-*tart* or (2*S*,3*S*)-*tart* ligands. In accordance with previous results, the tetranuclear anions incorporate the same enantiomers of the *tart* ligand [11]. The $\{V_4O_8\}$ group is composed of four $V=O_t$ groups that are bridged by four O_b atoms. The central $\{V_4O_4\}$ ring acquires an approximate boat conformation. All vanadium atoms are penta-coordinated, and the geometry of the coordination polyhedra can be described as square pyramids distorted toward trigonal bipyramids. The τ value ($\tau = 0$ for ideal square pyramid; $\tau = 1$ for ideal trigonal bipyramid [23]) is 0.3483 for V1, 0.3124 and 0.1972 for V2, 0.0863 for V3 and 0.1998 for V4. Each of the $\{VO_5\}$ pyramids contains one terminal oxygen atom (O_t), two bridging oxygen atoms (O_b), and two oxygen atoms from the tartrato ligand (O_h —from

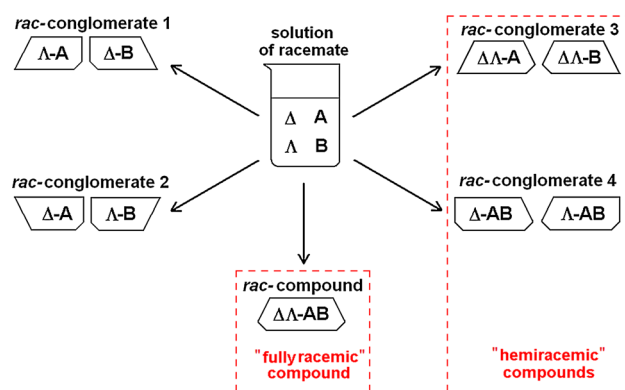
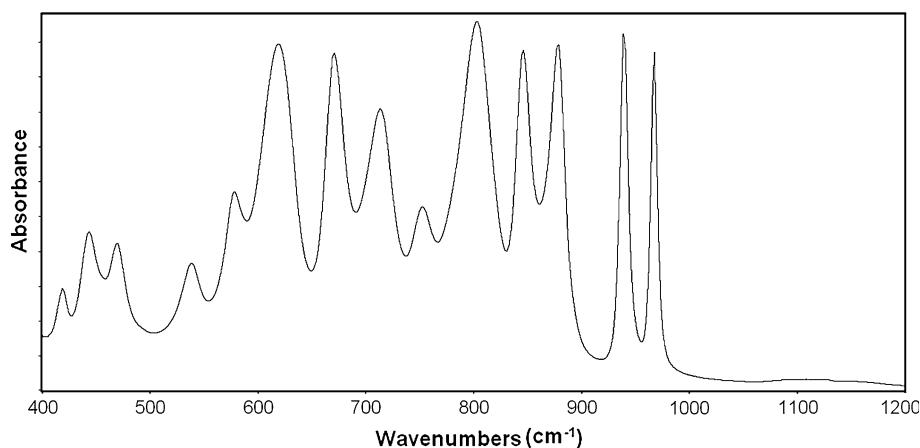


Fig. 7 The types of crystallization products from racemic solution containing both enantiomers of cation (Δ , Λ) and anion (A, B)

hydroxyl group and O_c —from carboxylate group). The bond lengths in the anion are within the expected ranges: 1.5782(34)–1.6053(32) (**1**), 1.5925(18)–1.6094(19) (**2**), 1.5937(19)–1.6081(19) (**4**) Å for $V=O_t$ bonds; 1.7671(31)–1.8701(32) (**1**), 1.7599(16)–1.8747(16) (**2**), 1.7696(17)–1.8813(16) (**4**) Å for $V-O_b$ bonds; 1.8535(39)–1.9506(33) (**1**), 1.8655(160)–1.9678(104) (**2**), 1.7932(53)–2.0052(104) (**4**) Å for $V-O_h$; 2.0288(33)–2.0719(33) (**1**), 2.0190(84)–2.0981(221) (**2**), 2.0154(98)–2.0742(44) (**4**) Å for $V-O_c$. The weak interactions between V and O atoms from the opposite pyramids [$d(V \cdots O) = 2.6407(31)$ and 2.5154(36), 2.7231(32) and 2.6602(36), 2.4684(30) and 2.4719(38), 2.5987(30) and 2.5903(30) (**1**), 2.5567(15), 2.4538(18), 2.6373(142), 2.7035(17) (**2**), 2.6131(15), 2.4576(15), 2.4535(114), 2.6371(16) (**4**) Å] complete the coordination polyhedra of the central atoms to strongly distorted octahedra. The tartrate anions are bonded as bis(bidentate) ligands and possess a *trans* conformation. The $[Fe(bpy)_3]^{2+}$ and $[Ni(bpy)_3]^{2+}$ cations have slightly distorted octahedral geometry with average bond lengths Fe–N 1.90–1.98 Å in **1** and **2** and Ni–N 2.07–2.10 Å in **4**.

Fig. 6 IR spectrum of $Ni(VO_3)_2$ in a KBr pellet



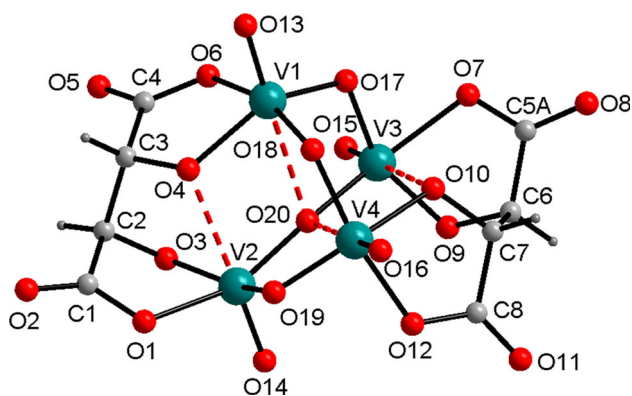


Fig. 8 Structure of the $[V_4O_8((2R,3R)\text{-tart})_2]^{4-}$ anion in **4**. Selected bond lengths (Å) [V1–O13, 1.6054(17); V1–O4, 1.9271(15); V1–O6, 2.0510(19); V1–O17, 1.7765(17); V1–O18, 1.9271(15); V2–O14, 1.5957(15); V2–O1, 2.0263(17); V2–O3, 1.8666(17); V2–O19, 1.8813(16); V2–O20, 1.8241(16); V3–O15, 1.5937(19); V3–O7, 2.0742(44); V3–O9, 1.7932(5); V3–O17, 1.8690(17); V3–O20, 1.8164(16); V4–O16, 1.6081(19); V4–O10, 2.0052(1); V4–O12, 2.0154(9); V4–O18, 1.8172(16); V4–O19, 1.7696(17)] and angles ($^\circ$) [O13–V1–O4, 109.587(8); O13–V1–O6, 93.302(8); O13–V1–O17, 106.985(9); O13–V1–O18, 101.629(8); O14–V2–O1, 100.451(8); O14–V2–O3, 99.706(8); O14–V2–O19, 103.306(8); O14–V2–O20, 102.62(8); O15–V3–O7, 99.117(1); O15–V3–O9, 99.010(2); O15–V3–O17, 103.699(9); O15–V3–O20, 102.934(8); O16–V4–O10, 109.524(3); O16–V4–O12, 97.087(3); O16–V4–O18, 101.017(8); O16–V4–O19, 107.526(9); V1–O17–V3, 112.044(9); V1–O18–V4, 128.029(9); V2–O20–V3, 170.972(9); V2–O19–V4, 112.589(9)]

The crystal structure of **1** is composed of three types of homochiral layers parallel to (100): (i) the layer consisting of $\Delta\text{-}[\text{Fe}(\text{bpy})_3]^{2+}$ cations; (ii) the layer consisting of $[V_4O_8((2R,3R)\text{-tart})_2]^{4-}$ anions, and (iii) the layer consisting of $\Lambda\text{-}[\text{Fe}(\text{bpy})_3]^{2+}$ cations (Fig. 9). The layers alternate in the order i–ii–iii–ii. The water molecules are distributed between the layers. In all presented structures, the layers consisting of $[M(\text{bpy})_3]^{2+}$ cations are homochiral irrespective of the configuration of the anions.

Compounds **2** and **4** are isostructural. The crystal structure of **4** is composed from the following layers: (i) the layer consisting of both enantiomeric forms of anions $[V_4O_8((2R,3R)\text{-tart})_2]^{4-}$ and $[V_4O_8((2S,3S)\text{-tart})_2]^{4-}$; (ii) layer consisting of $\Delta\text{-}[\text{Ni}(\text{bpy})_3]^{2+}$ cations; and (iii) layer consisting of $\Lambda\text{-}[\text{Ni}(\text{bpy})_3]^{2+}$ cations. The layers alternate in the order i–ii–i–iii (Fig. 10). The water molecules are distributed between the layers.

Some noteworthy $\pi\text{-}\pi$ interactions are present between the complex cations in the crystal structures of **2** and **4**. In the crystal structure of **2**, $\pi\text{-}\pi$ interactions between cations having different configurations are present. The interacting bipyridine planes are parallel, and the centroid to centroid distance is 3.77 Å. The second centroid to centroid distance (3.92 Å) is exceeding the limit suggested by Janiak [24]. In the crystal structure of **4**, two types of $\pi\text{-}\pi$

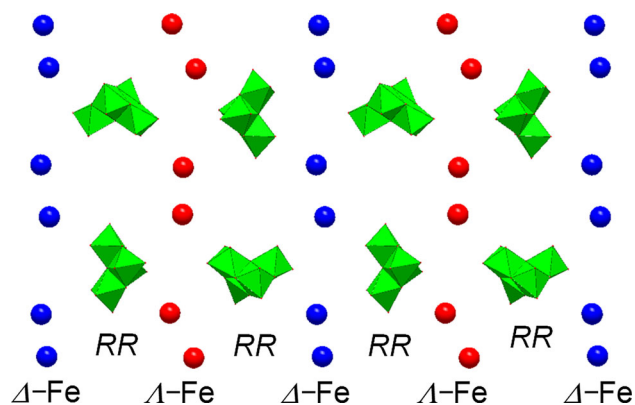


Fig. 9 Presentation of homochiral layers in structure of **1** ($\Delta\text{-Fe} = \Delta\text{-}[\text{Fe}(\text{bpy})_3]^{2+}$, $\Lambda\text{-Fe} = \Lambda\text{-}[\text{Fe}(\text{bpy})_3]^{2+}$, $RR = [V_4O_8((2R,3R)\text{-tart})_2]^{4-}$)

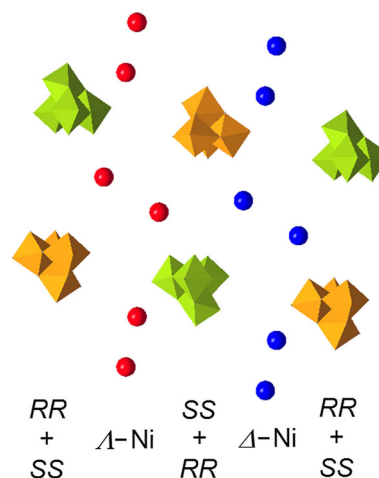


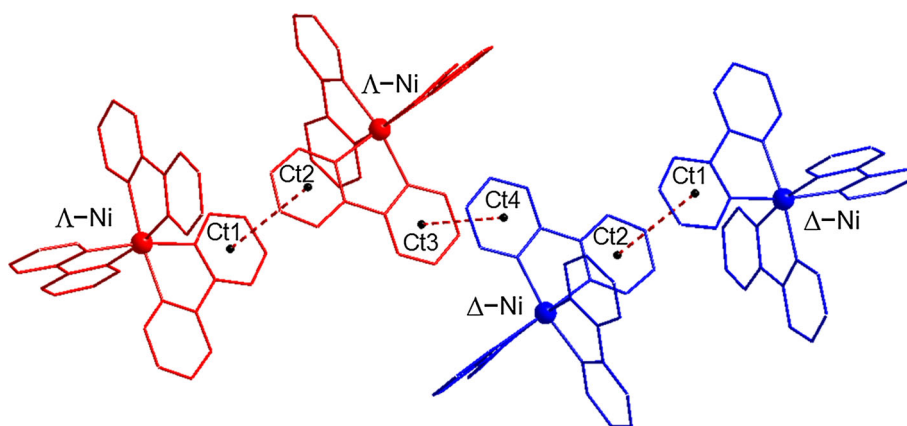
Fig. 10 Presentation of homochiral layers of cations (Δ and Λ) and heterochiral layers of anions ($RR + SS$) in the crystal structure of **4** ($\Delta\text{-Ni} = \Delta\text{-}[\text{Ni}(\text{bpy})_3]^{2+}$, $\Lambda\text{-Ni} = \Lambda\text{-}[\text{Ni}(\text{bpy})_3]^{2+}$, $RR = [V_4O_8((2R,3R)\text{-tart})_2]^{4-}$, $SS = [V_4O_8((2S,3S)\text{-tart})_2]^{4-}$)

interactions are present: (1) between bipyridine ligands of cations with the same configuration and (2) between bipyridine ligands of cations with different configuration (Fig. 11). The centroid to centroid distance between interacting bipyridine ligands are 3.83 and 3.77 Å in **4**. The angles between planes of interacting pyridine rings are 9.59° and 0.0° for **4**.

Supporting information

CCDC no. 1010531 (**1**) 1010532 (**2**) and 1010530 (**4**) contain supplementary crystallographic data. These data can be obtained free of charge from The Cambridge

Fig. 11 Presentation of π - π interactions in the crystal structure of **4**. Centroids are defined by following atoms: Ct1: N13, C19, C25, C26, C27, C28; Ct2: N22, C40, C41, C42, C43, C44; Ct3: N21, C39, C45, C46, C47, C48; Ct4: N21, C39, C45, C46, C47, C48



Crystallographic Data Centre via www.ccdc.cam.ac.uk/data_request/cif.

Acknowledgments This work was supported by the Ministry of Education, Science, Research and Sport of the Slovak Republic (Grant No. VEGA 1/0336/13).

References

- Breu J, Domel H, Stoll A (2000) *Eur J Inorg Chem* 2401–2408
- Gáliková J, Tatierysky J, Rakovský E, Schwendt P (2010) *Transit Met Chem* 35:751–756
- Breu J, Domel H, Norrby PO (2000) *Eur J Inorg Chem* 2409–2419
- Breu J, Seidl W, Huttner D, Kraus F (2002) *Chem Eur J* 8:4454–4460
- Huttner D, Breu J (2004) *Z Anorg Allg Chem* 630:2527–2531
- Breu J, Zwicknagel A (2004) *Z Naturforsch* 59b:1015–1025
- Antal P, Tatierysky J, Schwendt P, Gyepes R (2013) *J Mol Struct* 1032:240–245
- Tomíček O (1958) *Kvantitativní analyza (Quantitative analyses)*. SZN, Praha
- Spek AL (2003) *J Appl Crystallogr* 36:7–13
- Thornton DA, Watkins GM (1992) *J Coord Chem* 25:299–315
- Schwendt P, Tracey AS, Tatierysky J, Gáliková J, Žák Z (2007) *Inorg Chem* 46:3971–3983
- Nakamoto K (1986) *Infrared and Raman spectra of inorganic and coordination compounds*. Wiley, New York
- Braterman PS, Song JI, Peacock RD (1992) *Inorg Chem* 31:555–559
- Hadadzadeh H, Mansouri G, Rezvani A, Khavasi HR, Skelton BW, Makha M, Charati FR (2011) *Polyhedron* 30:2535–2543
- Palmer RA, Piper TS (1966) *Inorg Chem* 5:864–878
- González E, Rodrigue-Witchel A, Rebel C (2007) *Coord Chem Rev* 251:351–363
- Nazir R, Mazhar M, Wakeel T, Akhtar MJ, Siddique M, Nadeem M, Khan NA, Shah MR (2012) *J Therm Anal Calorim* 110:707–713
- Wang X, Heier KR, Stern CL, Poeppelmeier KR (1998) *Inorg Chem* 37:6921–6927
- Le Bail A, Lafontaine MA (1990) *Eur J Solid State Inorg* 27:671–680
- Pedregosa JC, Baran EJ, Aymonino PJ (1974) *Z Anorg Allg Chem* 404:308–320
- Müller-Buschbaum HK, Kobel MZ (1991) *Z Anorg Allg Chem* 596:23–28
- Lennartson A, Olsson S, Sundberg J, Håkansson M (2010) *Inorg Chim Acta* 363:257–262
- Addison AW, Rao TN, Reedijk J, van Rijn J, Verschoor GC (1984) *J Chem Soc Dalton Trans* 1349–1356
- Janiak C (2000) *J Chem Soc Dalton Trans* 3885–3896